TOWARDS ASSESSING SANDSTONE SURFACE MOISTURE AND DEGRADATION LEVEL FROM RADIOMETRICALLY CORRECTED TLS INTENSITY DATA

H. Laasch*, T. Medic, A. Wieser

Institute of Geodesy and Photogrammetry, ETH Zürich, Switzerland - (laaschh, tmedic, wiesera)@ethz.ch

KEY WORDS: LiDAR, Laser Scanning, Moisture Quantification, Intensity, Radiometric Correction, Cultural Heritage, Remote Sensing

ABSTRACT:

Water is a prevalent deterioration agent for historic masonry works, especially those made of clay-bearing sandstones. To preserve cultural heritage made of sandstone, it is important to monitor, and then detect the regions with water retention or stone deterioration. To that aim, we investigate the prospects of terrestrial laser scanner (TLS) intensities for quantifying moisture in sandstone. Through a series of experiments following the drying processes of sandstone samples, we verify that TLS intensities can serve as moisture proxies for remote-sensing water retention. We identify the theoretically most suitable wavelengths, systematic effects requiring mitigation, and promising mitigation strategies. However, we also observe that the intensities are significantly affected by the type of sandstone and its level of degradation. Our results indicate that it is possible to distinguish different sandstones and levels of artificial degradation by observing and analyzing TLS-intensity time series during the drying process.

1. INTRODUCTION

Many cultural heritage sites around the world are constructed from clay-bearing sandstone, which is susceptible to degradation from various mechanisms, resulting in substantial contour scales and slab-like damage as stones fall off the surface (Demoulin, 2016). Such damage probably originates from salt crystallization, water freezing, clay swelling or shrinking, atmospheric pollution or a mixture of the above (Praticò, 2020). These processes are all linked to changes in moisture levels on and within the sandstone, emphasizing the importance of detecting and monitoring moisture levels over time as a part of the preservation efforts. Agliata et al. (2018) categorize the methods for monitoring moisture into three classes: (1) destructive (requires a sample of the material), (2) nondestructive invasive (sensors are fixed inside of a probe), and (3) nondestructive noninvasive (through active or passive waves, e.g. magnetic field, infrared).

Given that it is usually desired not to damage heritage buildings, only non-destructive methods are suitable (Agliata et al., 2018). Among these methods, non-invasive remote sensing techniques offer high spatial resolution and coverage, making them beneficial for understanding the water flow within the surface. Lercari (2016) and Lemmens (2011, p. 101-121) present the advantages of using terrestrial laser scanners (TLS) instead of image-based methods for heritage preservation. A TLS is an active measurement system, not depending on external light conditions and shading. It allows for direct and accurate 3D shape reconstruction without the need for estimating camera poses and intrinsic parameters. Additionally, the laser beam intensity provides a measure of the surface reflectance, which is influenced by material properties (Kashani et al., 2015), such as moisture content.

Tab. 1 shows an overview of related relevant work aiming at estimating the moisture in man-made objects or rocks using TLS. These papers address the quantification of moisture for various materials using different instruments and estimation models. However, none of them investigated sandstone in particular or addressed the impact of different varieties of a certain material. Therefore, in this paper we evaluate the existing approaches and propose a new dedicated approach for estimating the humidity of sandstone. To achieve this, we conducted laboratory experiments tracking the drying process of different types of sandstone with different degradation levels. Our analysis of the intensity changes revealed that it is not possible to apply a single generalized model for accurately estimating the humidity of sandstone, as different types and degradation levels are associated with different functional relationships between laser intensities and moisture. However, we exploited these different intensity time series following the drying process and demonstrated that they can be directly used to determine the degradation levels and distinguish between types of sandstone. We further investigated all factors limiting the use of TLS intensities as unbiased moisture proxies, highlighting the main challenges and outlining some mitigation strategies.

The structure of the paper is as follows: In Sec. 2, we outline the measurement setup and provide details on our selection of TLSs, as well as the processing steps employed. Sec. 3 presents the experimental findings, with a primary focus on moisture estimation, followed by an examination of degradation levels. In Sec. 4 and 5, we give a more detailed discussion of effects underlying the processing steps and results from the earlier sections, and present mitigation strategies. Finally, we conclude the paper in Sec. 6 with a summary and a brief outlook.

2. METHODS

2.1 Experimental Setup

A laboratory experiment was set up to measure LiDAR intensities during the drying process of five different types of sandstone: Bentheim, Villarlod, Yellow Berne, Blue Berne, and Oberkirchen. From each stone type, we used one freshly cut, untreated sample and 1-2 samples that were treated with hydrochloric acid. This acid dissolves the calcium carbonate matrix

* Corresponding author

Reference	Application	Method	Instrument
Del Pozo et al. (2017)	Cultural heritage	Qualitative multispectral image classification	Faro Focus3D (905 nm), Riegl-Z390i (1550 nm), Canon EOS5D (400-700 nm), Mini-MCA6 (530-801 nm)
Hemmleb et al. (2006)	Construction	Qualitative moisture with index $NDMI = \frac{I_{ref} - I_{abs}}{I_{ref} + I_{abs}}$	Multispectral laser scanner with 980 nm (reference) and 1930 nm (absorption) wavelengths
Jin et al. (2021)	Beach moisture	Support Vector Regression to predict moisture	Riegl-VZ2000 (1550 nm)
Kaasalainen et al. (2010)	Building materials	Comparison between different sensors and the gravimetric moisture content	Leica ALS50-II (1064 nm), Fuji IS PRO (850 nm) and FARO LS880HE80 (785 nm)
Lerones et al. (2016)	Cultural heritage	Linear function with intensity corrected by specular reflectance, distance and histogram analysis	Leica HDS3000 (532 nm)
Tan et al. (2020)	Soil surface	Exponential model with distance and angle of incidence corrected intensity $M = a \cdot e^{b \cdot I_{corr}}$	Riegl VZ-4000 (1550 nm)
Themistocleous et al. (2020)	Cultural heritage	Quantitative moisture with index $LCI = \frac{I_{nir} - I_{blue}}{I_{nir} + I_{blue}}$	Canon SH260 (blue: 400-500 nm, NIR: 700-800 nm)
Vierhub-Lorenz et al. (2019)	Tunnel inspection	Qualitative moisture content with combination of the wavelengths $M = \frac{I_{ref} - I_{abs}}{I_{ref}}$	Multispectral laser scanner with 1320 nm (reference) and 1450 nm (absorption) wavelengths

Table 1. Overview of related relevant work.

of the stone, and the treatment thus simulates the degradation of the stone caused by (acidic) rain and air pollution (Zhang et al., 2021). The Bentheim and Oberkirchen samples were treated with an 8 % solution of the acid, while the other three were treated with a 4 % and 8 % solution. This was done because the 4 % solution had not caused any visible reaction for the former two types. All the samples had the same size of 8x8x2 cm^3. In the following text, they are named according to the type of sandstone and the concentration of acid used (e.g. Blue Berne 4a).

The specimens were initially wetted (submerged in water) until fully saturated and then left to dry for a total of 36 hours. We obtained reference values for the moisture content through weight changes observed using two Kern Pes 31000-1M balances. Two commercial TLSs were used to scan all sandstone samples simultaneously at five-minute intervals during the drying process from a distance of about 6 m. Specifically, these were a Leica RTC360 (RTC360) with a wavelength of 1550 nm and a Faro Focus3D S120 (S120) with a wavelength of 905 nm (see Sec. 2.2).

The experiment was conducted in a laboratory where air humidity and temperature were kept constant at 50 % and 20.6°C. To minimize uneven air circulation (increased close to the air ventilation duct), the sandstone samples were placed inside a box that was open on one side only, as shown in Fig. 1. The samples were placed at an angle of 30 degrees relative to the scanner's line of sight to avoid an impact by specular reflection which can cause signal saturation and bias in the intensity values. Two Spectralon reflection standards, with 5 % and 80 % reflectivity, respectively, were placed at the side of the box to monitor eventual laser intensity variation over time.

To ensure the repeatability of the results, we independently recorded two time series of weight and TLS measurements for each sample. This shows not only the repeatability of the single measurements but also the repeatability of the drying process (see Sec. 4.2).

Figure 1. Experimental setup.

2.2 Choosing Scanners Based on Their Wavelengths

Light at different wavelengths is absorbed differently by liquid water (Curcio and Petty, 1951). When scanning wet sandstone surfaces the absorption depends on the joint effect of moisture and surface. To determine which wavelengths are absorbed

more by wet sandstone, spectrometer measurements were conducted using a PANalytics FieldSpec4 Standard-Res point spectrometer and a THORLABS SLS201L/M light source in a dark environment. Fig. 2 shows the ratio between the spectral profiles (reflectance in the range of 350 nm - 2500 nm) of the dry and wet stone for each sample. Based on these measurements, there is a clear difference in reflectance (factor 2.5 or higher) at all tested wavelengths between about 500 and 2250 nm, but light with wavelengths around 1450 nm and 1940 nm, two of the known absorption bands of liquid water, is more sensitive to water content in sandstone than light with other wavelengths. Therefore, using a TLS with a wavelength within these absorption peak areas would be ideal. While such scanners are currently not commercially available, a wavelength of 1550 nm is commonly used for TLSs, and we expected such scanners to be suitable for our investigation. Fig. 2 suggests that the sensitivity with respect to moisture would be still slightly higher at this wavelength than at other wavelengths found in current TLSs.

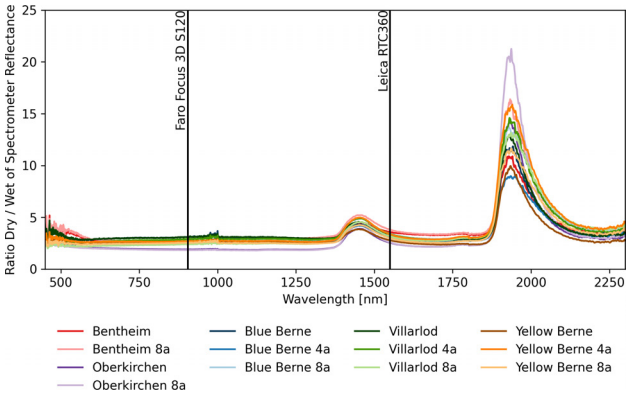

Figure 2. Ratio of spectrometer measurements between wet and dry sandstone samples.

Based on these insights, we chose an RTC360 (1550 nm) and an S120 (905 nm) from the pool of available TLSs for monitoring the drying process. The intention was to investigate if generating spectral indices, as intensity ratios of a more (RTC360) and less (S120) sensitive TLS (see Fig. 2), would allow for a more accurate estimation of moisture content in sandstone. Computing correlations between the weight measurements, as a proxy for moisture content, and intensities confirmed that the observations at 1550 nm wavelengths are more sensitive than at 905 nm wavelength. However, the difference of the correlation coefficients was very small (-0.97 vs. -0.95), as also visible in Fig. 2. Hence, the choice of the adequate instrument can be relaxed, and both instruments selected in this study are equally suited. Their sensitivity with respect to water on the surface is too similar to benefit from a spectral index calculated from the intensity values of both instruments. Therefore, in Sec. 3 we present only the results for the RTC360.

2.3 Data Pre-Processing

The intensity measurements are influenced, among others, by geometrical, instrumental, and temporal effects, as explained in Sec. 4. To ensure that the results are not contaminated by these factors, pre-processing of the intensities is needed (see Fig. 3).

In a first step, the intensity values have to be transformed from scanner specific values into values representing the reflectance. This correction of the intensity scale is achieved using a scanner-dependent functional model (see Sec. 4.4). For each

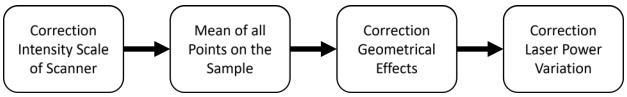

Figure 3. Pre-processing steps.

sandstone and Spectralon sample (Fig. 1) we then calculated the mean intensity and standard deviation over all ($\sim$1000) data points on the sample for each time point (every 5 min over 36 h).

To reduce the geometrical effects and thus allow comparison of samples scanned at different distances or angles, calculating intensity corrections would be required (Kaasalainen et al., 2011; Pfeifer et al., 2008). Since the distances and angles of incidence were (on purpose) not changed during the experiments reported herein, we chose a simplified approach. Before wetting the samples and starting the previously mentioned scans, we placed the 80 % Spectralon consecutively on the position of each sample inside the box (Fig. 1, Sandstone samples' locations), scanned, and used the intensity data from these scans to later convert intensities into reflectivities. This was done by computing the ratio of the known Spectralon reflectivity (0.8) and the observed Spectralon intensity (mean over the Spectralon plate) and applying it as a scale factor to all sample intensities (one constant scaling factor per position in the box). This way we accounted implicitly for the systematic influences of the geometric configuration without the need for an explicit functional model.

To correct for temporal laser power variation (see Sec. 4.3) the comparable approach was applied on top of the previous correction. For this, we introduced an additional scaling factor computed as a ratio of the known Spectralon reflectivity (0.8) and mean intensity over the Spectralon plate that was present in each scan during the drying process (Fig. 1, bottom left corner of the box). Hence, each scan, i.e. each timestamp, received own second scaling factor that was applied to the reflectivity values of all point cloud points computed by the previous correction step. In the following sections, we use the term "mean intensity" for such per-sample-averaged and corrected intensity values of the reflected laser beam.

To obtain the reference data point for completely dry sandstone, we dried the samples in an oven with air circulation at 65°C until the weight changed by no more than 0.1 % in 24 hours. The difference between the measured weight during the drying process and the dry weight allowed us to calculate the amount of water inside the sandstone sample. Although this relative water content (RWC) is an integral over the whole stone, we used the measure as a reference for the surface moisture in Sec. 3, because the samples are small.

3. RESULTS

3.1 Relation Between Intensity and Relative Water Content

Fig. 4 shows the relationship between the intensity and RWC over the drying process. It is observable that the curves differ regarding their scale, shape, and extreme values for each sandstone type and level of degradation. However, some generalizable characteristics exist. When the stone is drying, the intensity increases. Additionally, the curves are almost flat (horizontal) on both extremes, indicating that the intensity cannot

represent the changes in RWC well when the stone has either very little or very much water inside. This may be related to non-uniform humidity distribution in these cases.

The calculated RWC provides a measure for the entire sample. Thus, the flat parts of the curve could be explained by the following drying processes: First, at the beginning of the drying process, as surface water evaporates, the water from inside the stone moves towards the surface due to capillary phenomena or pressure gradients (Pichler et al., 2022). As a result, even though the stone's overall water content is reduced (affecting weight measurements), the surface of the sample retains the same moisture. This leads to unchanged intensity, since the laser light is mainly back-scattered by the surface of the sandstone. A comparable phenomenon occurs at the end of the drying process, when the stone approaches its equilibrium moisture content. At this point, the intensity could be unchanged, if the surface is already at its equilibrium, while there is still excess moisture inside the stone that slowly exits the sample.

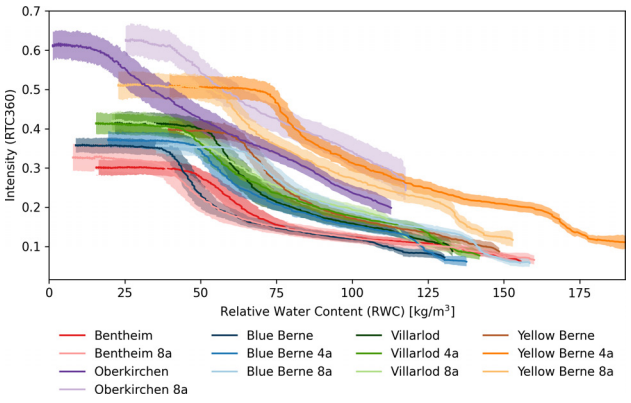

Figure 4. Mean intensity (see Sec. 2.3) vs. RWC of sandstone samples while drying (semi-transparent patches = standard deviations of single intensity measurements).

All of these effects depend on the size of the capillaries and the material properties of the sandstone, which can cause differences in the shapes of the drying process curves. Additionally, the curves differ because each sandstone has unique surface properties, e.g. color and roughness, resulting in different reflectivity, as well as different water retention properties, resulting in different maximum water content. Hence, to accurately estimate the RWC from intensity measurements, it is necessary to know the sandstone type and level of degradation and to use this information to calibrate the intensity-RWC response curve.

However, a benefit of these differentiating effects is that they allow for the categorization of different sandstones. This enables detecting degraded sandstone patches among "healthy" ones if data series of monitoring such drying processes are available.

3.2 Degradation Level of Sandstone

To better highlight this phenomenon, Fig. 5 represents the normalized drying process curves (min-max normalization for both intensity and RWC of each curve) for all samples. Again, we can observe that such simple data transformation cannot eliminate all the differences between the curves. However, we can observe a largely generalizable feature related to stone degradation, apparent between the solid and dashed lines approximately in the middle of the drying process. 7 out of 8 curves of acid-treated samples (dashed) are flatter than 4 out of 5 non-treated samples (solid) in the region of 0.3 and 0.8 normalized RWC. There are two outliers: the Bentheim 8a and the Oberkirchen samples, which have almost unchanged trends irrespective of the acidity treatment. A reason could be, that those two types of sandstones did not react as well as the others to the treatment. Besides that, the grain size is much smaller for these two types relative to the others, which could impact the drying process.

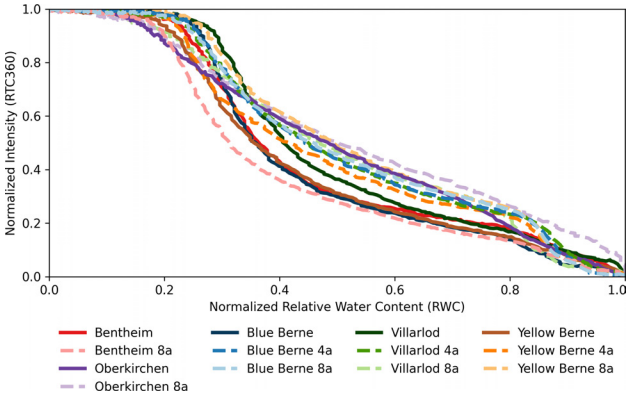

Figure 5. Mean intensity vs. RWC of sandstone samples (normalized by min-max scaling to 0-1 per sample).

Fig. 6 shows that different degradation levels cause distinct changes in the drying process. Polynomials of the 9th degree were fitted to six intensity-RWC curves of a single sandstone type (2x Villarlod, Villarlod 4a, Villarlod 8a) and resulted with a mean R^2 of 0.99. The 1st derivatives of these functions are presented in Fig. 6. They show that the minimum of these derivatives, i.e., the steepest slope of the normalized intensity versus RWC curve, is related to the concentration of hydrochloric acid used, which in turn corresponds to the degradation level. Furthermore, Fig. 7 indicates, that it is possible to regress the degradation level of sandstone with a R^2-value of 0.90. However, confirming these observations and assessing their generalizability requires further investigation. Additionally, for later real world applications precipitation, humidity of the air, temperature and radiation may have to be taken into account, and the model will have to be fitted to the intensity-time-relationship because the weight cannot be measured.

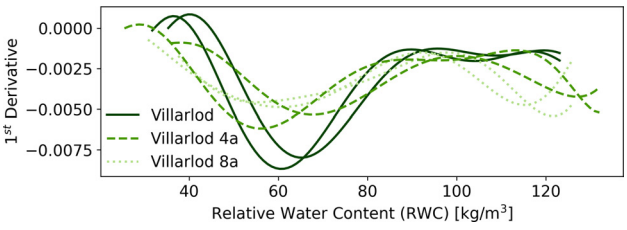

Figure 6. 1st derivative of the polynomial function fitted to the curves in Fig. 4 (1 sandstone type, 3 degradation levels, 2 repetitions).

4. TOWARDS ACCURATELY ESTIMATING MOISTURE USING INTENSITY

As presented in Sec. 3.1, various factors can affect the intensity measurements. The intensity can thus change even if the properties of the sandstone, e.g., its moisture content, remain constant. The influence of some of these factors can be reduced by employing adequate measurement strategies (see Sec. 5).

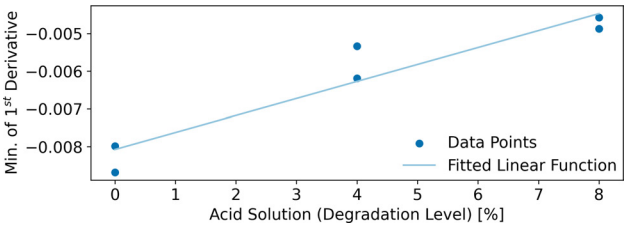

Figure 7. Minimum of the curves in Fig. 6 vs. acid concentration (degradation level).

However, when such strategies are not applicable, or they are shown to be insufficient, the relationship between the influencing factor and the intensity needs to be modeled and the intensity value corrected. Alternatively, the influences need to be quantified as part of the uncertainty budget.

Overall, the factors can be classified into four main categories (Kashani et al., 2015): (i) instrument-dependent factors, such as the type of photodiode and its resolution; (ii) geometry-dependent factors, such as measurement distance or angle of incidence (AOI); (iii) time-dependent factors, such as warm-up effects and other temporal variations of the laser power; and (iv) object-dependent factors, such as surface roughness and reflectivity pattern. A more detailed discussion of all factors that we recognized as significant in our work and their relevance for estimating moisture in sandstone are provided in the following subsections.

4.1 Noise of Intensity Measurements

It is important to consider the precision of acquired intensity values, as it defines the maximal sensitivity of moisture measurements. The precision of the intensity measurements (Gaussian distributed) depends on the scanner used and on the power of the back-scattered light, or the intensity itself, in a not necessarily linear manner, see Pfeifer et al. (2007). For the S120 with the raw intensity values between 0 and 1, we found an empirical standard deviation of about 0.002 for the intensity values across a homogeneous area with 80 % reflectance scanned at 6 m distance, and 0.005 for an area with 5 % reflectance. In contrast, the RTC360 has a higher empirical standard deviation of 0.025 for 80 % reflectance, and 0.003 for 5 % reflectance.

The intensity changes during the drying process are on average 0.32 for the RTC360 and 0.21 for the S120. Therefore, the noise relates to 4.3 % of overall change for the RTC360 and 1.5 % for the S120. These values present the best achievable precision of moisture estimation for the single-point measurements when all systematic effects are eliminated. However, spatial averaging can be used to increase this precision at the expense of reduced spatial resolution (as done in our experiments).

4.2 Repeatability of Drying Patterns

The repeated drying processes for the samples yielded similar but statistically different results, see Fig. 8 as an example. Plausible reasons for this can be small differences in the climatic conditions in the lab, leading to changes in the drying pattern. Additionally, the empirical standard deviation (σ) of the mean intensity is likely a too optimistic measure of the uncertainty as it ignores spatial correlations between the single-point measurements, and the impacts of systematic deviations not sufficiently compensated using the approaches mentioned in Sec. 2.3.

Because of these observations, it is apparent that the transfer of the results and conclusions presented in Sec. 3 to the real-world application will be challenging. It will require an understanding of the relationship between the atmospheric conditions and changes in the drying process. For example, if the air humidity is very low, the surface dries faster than if the air humidity is high.

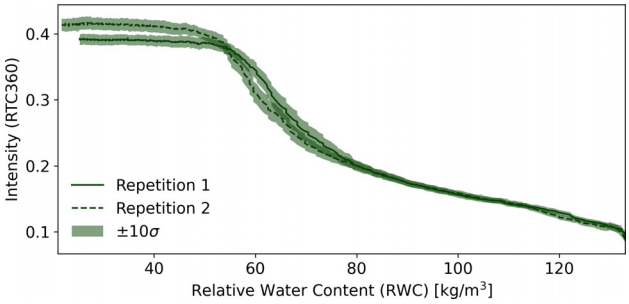

Figure 8. Intensity vs. RWC in the untreated Villarlod sample of two drying repetitions (standard deviations of the mean intensity scaled for better visibility).

4.3 Laser Power Variation – Long Term Drifts

The intensity depends on the power of the emitted signal, which can vary over time, thus leading to fluctuations in recorded intensity (see Fig. 9). Furthermore, temperature changes, particularly during the warm-up phase of the instrument, can affect the intensity values. E.g., for the S120 scanner, we observed intensity changes during warm-up corresponding to 70 % of the whole changes during the drying process, and still fluctuations of about 6 % during the rest of the 36 hrs. It is advisable to discard the data collected during the warm-up phase of the instrument, which lasts approximately 30-60 min (see Fig. 9) with the scanners used herein, which corresponds to the warm up effect on the geometry (Medić et al., 2021). If a target of stable reflectance can be placed in the scanned scene, it is also possible to the temporal variability numerically, as described in Sec. 2.

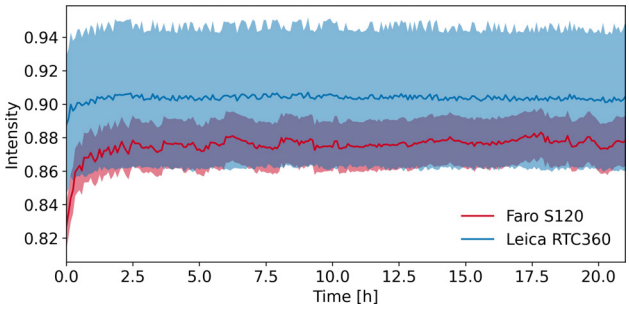

Figure 9. Mean intensity of Spectralon (80 % reflectance) over time (semi-transparent patches = standard deviation of single observations).

4.4 Intensity Scale of Scanners

TLSs differ in transmitted energy and some have additional features such as brightness reducers, automatic gain controls, or amplifiers to handle weakly reflective surfaces (Kashani et al., 2015). Due to all these factors, the recorded intensity may not have a simple e.g., linear, relation to the reflectivity of the scanned surfaces. If this relation is not provided by the scanner manufacturer, it can be established empirically by scanning

different surfaces with known reflectivity, e.g. Spectralon, and fitting a suitable function to the data.

In our work, we made such measurements for both scanners using five different reflectivity standards (5, 25, 60, 80, and 99 %). For the S120 scanner, the relationship can be modeled by a logarithmic function $R = a \cdot log(b \cdot I_m)$, for the RTC360 by a linear function $R = a + b \cdot I_m$, where I_m represents the measured intensity, R represents the reflectivity, and a and b are the model parameters (see Fig. 10). For the S120 scanner we chose a logarithmic function over linear one due to higher R^2 value. Using these (distance- and AOI-independent) models, it is possible to establish functional relationships between reflectivity and intensity, making the observations of different scanners comparable. This is especially important if the measurements of two different scanners are integrated for a single project, e.g. to compute spectral indices (see Sec. 5). To conclude, in order to have a generalizable model for the RWC estimation, it is necessary to adjust the intensity scales, as they impact the RWC-intensity relationship.

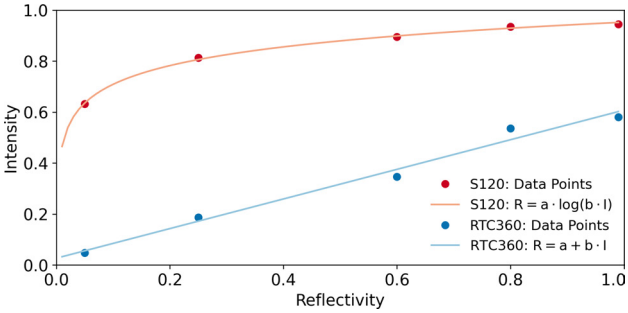

Figure 10. Intensity vs. reflectivity of 5 Spectralon plates for 2 scanners.

4.5 Distance and Angle of Incidence

The intensity typically decreases exponentially with distance (Wagner, 2010; Kaasalainen et al., 2011). However, at close distances (up to about 10 m), the intensity-distance relation is no longer exponential due to instrumental effects, such as those caused by the beam waist and detector aperture (Kaasalainen et al., 2011; Pfeifer et al., 2007). To account for these effects, manufacturers use the own instrument-specific correction functions for the distance dependence (see Fig. 11), that is given with the LiDAR equation (Pfeifer et al., 2008).

As Fig. 11 shows for S120 scanner, the manufacturer's correction does not eliminate the change of intensity values with distance completely. Especially in close ranges, the intensities vary by 0.1 in value, which corresponds to about 60 % in RWC change. Hence, unbiased RWC estimation requires accounting for this effect, even in the case of using intensity values which include the manufacturer's default corrections.

According to the LiDAR equation, the intensity of a laser beam is directly proportional to the cosine of the AOI (Pfeifer et al., 2008), which holds only for perfectly Lambertian surfaces. However, in reality, the relationship between intensity and AOI varies significantly depending on the surface roughness and reflectance of the object being measured (see Fig. 12). For instance, when measuring a sample of Villarlod sandstone with a smooth surface, AOIs smaller than 0.1 rad can produce high intensities that result from specular reflectance. This effect can bias the RWC estimates and needs to be accounted for.

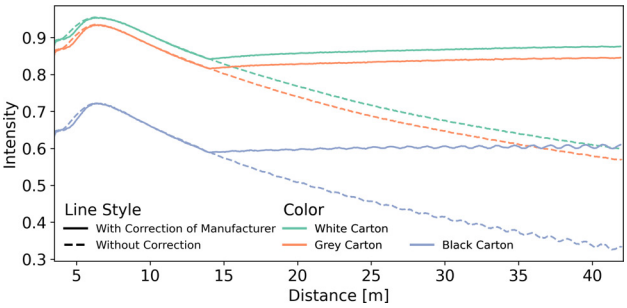

Figure 11. Distance-Intensity-Dependency with and without the correction by the manufacturer (firmware-update) and visible cyclic deviations in low intensities for the laser scanner S120.

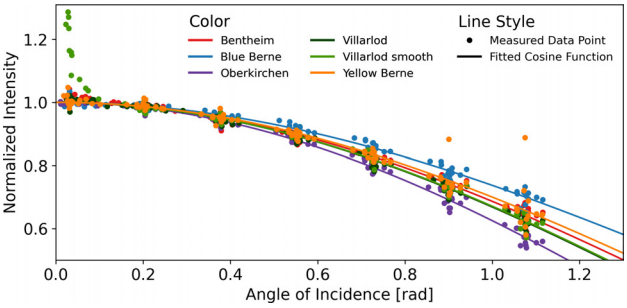

Figure 12. Angle-of-incidence versus intensity relation for an RTC360 and different sandstone samples.

The Oberkirchen sandstone has a very fine granularity, whereas the Blue Berne has a much coarser granularity. As shown in Fig. 12, the stone with the finer granularity exhibits a greater decrease in the power of back-scattered light with the decrease of AOI. Moreover, the slope of the curve modeling the AOI effect is found to be distance-dependent in our data, with greater distance resulting in higher curvature, as illustrated in Fig. 13. This observation does not follow the data reported in the literature and needs to be further investigated. It is possible that this can be explained by the changes in relative proportion between the sandstone particles and laser beam footprint sizes, due to the increase in footprint with the distance. Nevertheless, these differences in functions modeling intensity and AOI relationship can reach magnitudes of 0.05 for an AOI of 60° for different types of sandstones, which is up to 16 % of the overall RWC change during the drying process. For the difference caused by the distance, the effect is smaller and equals about 5 % of the overall RWC change. Hence, these effects can significantly bias the results, especially if the measurements are taken at higher AOIs. Moreover, at very small AOIs the specular reflectance has a large influence on the intensity. To minimize these effects, we recommend using measurements taken at AOIs in the range of 10° to 30° for estimating the RWC.

4.6 Cyclic Deviations

Due to multipath effects within the instrument, the measurements exhibit cyclic errors (Covell and Rüeger, 1982). These effects have primarily been analyzed concerning distance measurements, as shown in Lichti and Licht (2006), Dorninger et al. (2008) and Wieser et al. (2022). However, as the phasor model presented in Covell and Rüeger (1982) demonstrates, they also affect intensity. Fig. 11 shows that the cyclic deviations in intensity values of the S120 scanner depend on both distance and the power of the back-scattered signal.

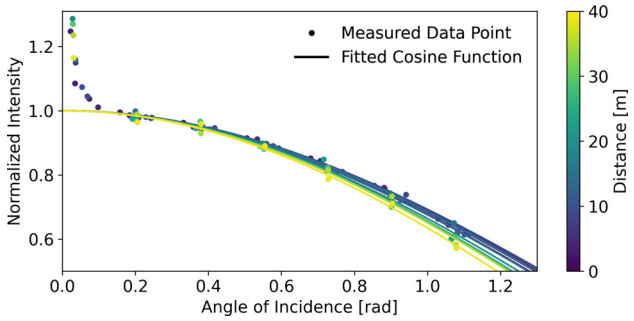

Figure 13. AOI-Intensity-Dependency at different distances for the Villarlod sample with small surface roughness.

Therefore, in the context of the drying process, the effect of the cyclic deviations is larger when the sandstone is wet due to its low reflectivity. When the sandstone is drying, the reflectance gets higher and therefore the effect of the cyclic deviation is decreasing. Moreover, the exact impact of this effect (magnitude and sign) depends on the distance. For the analyzed scanner (S120), we found changes of up to 0.003 in intensity value resulting from cyclic deviations, depending on the reflectivity of the sample and the distance. This change is about 1.3 % of the whole change in RWC during a drying process, which is at the same level as the noise of the individual measurements. Hence, cyclic deviations should be accounted for primarily when demands towards RWC estimation accuracy are rigorous.

4.7 Material Properties

The material properties relevant for the RWC estimation were discussed in detail in Sec. 3. They primarily influence the reflectance and laser beam penetration depth, both of which can change as the stone dries. To summarize, the noise level, the corrections for distance, AOI, and cyclic deviations, as well as the drying process curves, all depend on these material properties. Hence, the intensity-vs-RWC curve of the material needs to be known in advance for unbiased RWC estimation.

5. STRATEGIES FOR MITIGATING CHALLENGES IN MOISTURE ESTIMATION

The previous section discussed factors influencing the intensity values that we found relevant for the RWC estimation in sandstone. The influence of many of them can be observed in controlled conditions and later functionally modeled and removed from observed intensity values. However, for some of them, this is not sufficient or there are measurement strategies that could replace these cumbersome procedures. Following, we discuss further challenges and possible mitigation strategies required for accurately estimating the RWC from intensity values.

A-priori knowledge of all intensity-RWC response curves is necessary to estimate the RWC. Knowing the intensity-RWC relationship over the whole range of values, it is possible to estimate the RWC with an accuracy that is primarily limited by the repeatability of the drying process presented in Sec. 4.2. If only the extremes of the curves are known a priori, the intensities over the drying process can be normalized and the RWC can still be estimated (see Fig. 5), however, with reduced accuracy, as we do not account for the differences between the different degradation levels and sandstone types.

The wavelengths have different intensity dependence on moisture change (see Fig. 2). Hence, by using a combination (spectral index) of a wavelength with low moisture dependency (e.g. 600 nm-1350 nm) and another one with high dependency (e.g. 1450 nm or 1930 nm), the impact of different material properties, such as stone types and levels of degradation can be reduced, but not completely removed. Different ratios of maximally and minimally dependent wavelengths demonstrated in Fig. 2 (e.g. Oberkirchen 8a having a noticeably larger difference between min and max value from the rest) highlight that using the spectral index cannot guarantee a completely unbiased estimation of the moisture content. Further investigations have to be done to verify these observations.

Using two different wavelengths can also mitigate systematic effects related to measurement geometry and instrument characteristics, provided that the object's reflectance is comparable for both wavelengths except for the impact of humidity. A dual-frequency TLS such as the one in Vierhub-Lorenz et al. (2019) can achieve this. However, our attempt of using two different commercial TLSs (RTC360 and S120) for this purpose yielded poor results due to the presence of different systematic effects between the scanners that could not be canceled out by generating the difference or ratio. Additionally, both scanners were similarly sensitive to moisture, causing a poor signal-to-noise ratio of the moisture index based on their intensities. Assessing whether better mitigation of systematic effects allows successfully using this dual-wavelength strategy with pairs of commercial scanners or requires a dual-/multi-wavelength scanner is left for further research.

6. CONCLUSION

In this study we investigated the feasibility of using the intensity values of a commercial terrestrial laser scanner (TLS) to estimate the relative water content (RWC) of sandstone. As a part of our efforts, we identified and quantified systematic effects influencing intensities that require mitigation for unbiased RWC estimation and we proposed a promising mitigation strategy.

We carried out experiments that followed the drying process of sandstone samples of different types and levels of degradation (induced by hydrochloric acid). These experiments showed that the intensity-RWC-response curve depends both on stone type and degradation level. Hence, without prior knowledge of these factors, it is not possible to establish an accurate relationship between TLS intensities and moisture. We demonstrated that for each type and degradation level, a functional relationship can be modeled well with a polynomial of the 9th degree (mean R^2 of 0.99). By analyzing the shape of the intensity-RWC-response curve it is possible to discriminate between degraded and "healthy" sandstone. Moreover, our initial results suggest that the minimum values of the 1st derivatives of these functions could even be used to quantify the level of sandstone degradation. However, it is necessary to further investigate whether these observations can be generalized.

In conclusion, the overall goal of estimating the RWC from TLS intensity data is achieved, but prior knowledge of sandstone type and level of degradation is needed, and corrections to mitigate other effects have to be applied. Our future research will be focused on extending the present approach to also use the RGB images provided by modern TLS, and on transferring the approach to outdoor application in real use cases of monitoring cultural heritage buildings made of sandstone.

ACKNOWLEDGMENTS

This work was supported by an ETH Research Grant. Anjo Weichbrodt and the Chair of Physical Chemistry of Building Materials (ETH Zürich) provided the sandstone samples, the scales, and domain knowledge in cultural heritage preservation.

References

Agliata, R., Mollo, L., Greco, R., 2018. Moisture measurements in heritage masonries: a review of current methods. *Material Evaluation*, 76, 1468–1477.

Covell, P. C., Rüeger, J. M., 1982. Multiplicity of Cyclic Errors in Electro-Optical Distance Meters. *Survey Review*, 26(203), 209–224.

Curcio, J. A., Petty, C. C., 1951. The Near Infrared Absorption Spectrum of Liquid Water. *Journal of the Optical Society of America*, 41(5), 302.

Del Pozo, S., Rodríguez-Gonzálvez, P., Sánchez-Aparicio, L. J., Muñoz-Nieto, A., Hernández-López, D., Felipe-García, B., González-Aguilera, D., 2017. Multispectral Imaging in Cultural Heritage Conservation. *The International Archives of the Photogrammetry, Remote Sensing and Spatial Information Sciences*, XLII-2/W5, 155–162.

Demoulin, T., 2016. Durability of clay-bearing sandstone and its repair by viscoelastic mortars. PhD thesis, ETH Zurich.

Dorninger, P., Nothegger, C., Pfeifer, N., Molnár, G., 2008. On-the-job detection and correction of systematic cyclic distance measurement errors of terrestrial laser scanners. *Journal of Applied Geodesy*, 2(4).

Hemmleb, M., Weritz, F., Schiemenz, A., Grote, A., Maierhofer, C., 2006. Multi-Spectral Data Acquisition and Processing Techniques for Damage Detection on Building Surfaces. *Image engineering and vision metrology*, 6.

Jin, J., Verbeurgt, J., De Sloover, L., Stal, C., Deruyter, G., Montreuil, A.-L., Vos, S., De Maeyer, P., De Wulf, A., 2021. Support vector regression for high-resolution beach surface moisture estimation from terrestrial LiDAR intensity data. *International Journal of Applied Earth Observation and Geoinformation*, 102, 102458.

Kaasalainen, S., Jaakkola, A., Kaasalainen, M., Krooks, A., Kukko, A., 2011. Analysis of Incidence Angle and Distance Effects on Terrestrial Laser Scanner Intensity: Search for Correction Methods. *Remote Sensing*, 3(10), 2207–2221.

Kaasalainen, S., Niittymaki, H., Krooks, A., Koch, K., Kaartinen, H., Vain, A., Hyyppa, H., 2010. Effect of Target Moisture on Laser Scanner Intensity. *IEEE Transactions on Geoscience and Remote Sensing*, 48(4), 2128–2136.

Kashani, A., Olsen, M., Parrish, C., Wilson, N., 2015. A Review of LIDAR Radiometric Processing: From Ad Hoc Intensity Correction to Rigorous Radiometric Calibration. *Sensors*, 15(11), 28099–28128.

Lemmens, M., 2011. *Geo-information*. Springer Netherlands.

Lercari, N., 2016. Terrestrial Laser Scanning in the Age of Sensing. M. Forte, S. Campana (eds), *Digital Methods and Remote Sensing in Archaeology*, Springer International Publishing, 3–33.

Lerones, P. M., Vélez, D. O., Rojo, F. G., Gómez-García-Bermejo, J., Casanova, E. Z., 2016. Moisture detection in heritage buildings by 3D laser scanning. *Studies in Conservation*, 61(sup1), 46–54.

Lichti, D. D., Licht, M. G., 2006. Experiences With Terrestrial Laser Scanner Modelling and Accuracy Assessment. *Int. Arch. Photogramm. Remote Sens. Spat. Inf. Sci*, 36(5).

Medić, T., Kuhlmann, H., Holst, C., 2021. A priori vs. in-situ terrestrial laser scanner calibration in the context of the instability of calibration parameters. *Contributions to International Conferences on Engineering Surveying*, 128–141.

Pfeifer, N., Dorninger, P., Haring, A., Fan, H., 2007. Investigating terrestrial laser scanning intensity data: quality and functional relations. *International Conference on Optical 3-D Measurement Techniques VIII*, 328–337.

Pfeifer, N., Höfle, B., Briese, C., Rutzinger, M., Haring, A., 2008. Analysis of the Backscattered Energy in Terrestrial Laser Scanning Data. *Int. Arch. Photogramm. Remote Sens. Spat. Inf. Sci*, 37, 1045–1052.

Pichler, C., Lackner, R., Bader, T., Perfler, L., 2022. Water vapor diffusion properties of Obernkirchener sandstone: Analysis of DVS data. *Construction and Building Materials*, 347, 128554.

Praticò, Y., 2020. Practical applications of science for the conservation of built heritage: Strategies based on the analysis of rare events. PhD thesis, ETH Zurich.

Tan, K., Chen, J., Zhang, W., Liu, K., Tao, P., Cheng, X., 2020. Estimation of soil surface water contents for intertidal mudflats using a near-infrared long-range terrestrial laser scanner. *ISPRS Journal of Photogrammetry and Remote Sensing*, 159, 129–139.

Themistocleous, K., Evagorou, E., Mettas, C., Prodromou, M., Hadjimitsis, D. G., 2020. The documentation of cultural heritage sites in Cyprus using integrated techniques: the case study of the Church of Agios Athanasios and Kyrillos. *Eighth International Conference on Remote Sensing and Geoinformation of the Environment (RSCy2020)*, SPIE, 73.

Vierhub-Lorenz, V., Predehl, K., Wolf, S., Werner, C. S., Kühnemann, F., Reiterer, A., 2019. A multispectral tunnel inspection system for simultaneous moisture and shape detection. *Remote Sensing Technologies and Applications in Urban Environments IV*, SPIE, 32.

Wagner, W., 2010. Radiometric calibration of small-footprint full-waveform airborne laser scanner measurements: Basic physical concepts. *ISPRS Journal of Photogrammetry and Remote Sensing*, 65(6), 505–513.

Wieser, A., Balangé, L., Bauer, P., Gehrmann, T., Hartmann, J., Holst, C., Jost, B., Kuhlmann, H., Lienhart, W., Maboudi, M. et al., 2022. Erfahrungen aus einem koordinierten Vergleich aktueller Scanner. *DVW e. V.(Hrsg.): Terrestrisches Laserscanning*, 23–38.

Zhang, J., Li, Z., Li, L., Liu, J., Liu, D., Shao, M., 2021. Study on weathering mechanism of sandstone statues in Southwest China: example from the sandstone of Niche of Sakyamuni Entering Nirvana at Dazu Rock Carvings. *Natural Hazards*, 108(1), 775–797.